Received October 1995
Revised August 1996
Accepted December 1997

# Thermoconvective flow in a saturated, isotropic, homogeneous porous medium using Brinkman's model: numerical study

Ò. À. Bèg
*Structural Engineering Group , Ove Arup & Partners, Consulting Engineers, Manchester, UK*
H.S. Takhar
*School of Engineering, Manchester University, Manchester, UK*
V.M. Soundalgekar
*31A-12 Brindavan Society, Thane, Bombay, India, and*
V. Prasad
*School of Engineering, State University of New York at Stony Brook, New York, USA*

## Nomenclature

| | | |
|---|---|---|
| $f$ | = | dimensionless stream function |
| $u,v$ | = | velocities along x, y directions |
| $g$ | = | acceleration due to gravity |
| $k$ | = | thermal conductivity |
| $C_p$ | = | specific heat at constant pressure |
| $T$ | = | temperature |
| $U_0$ | = | reference velocity |
| $U_\infty$ | = | free stream velocity (at edge of boundary layer) |
| $T_w, T_\infty$ | = | wall temperature, free stream temperature |
| $Ec$ | = | Eckert number $\frac{U_0^2}{C_p \Delta T}$ |
| $Gr$ | = | Grashof number $\frac{g\beta\Delta T L^3}{\nu^2}$ |
| $Pr$ | = | Prandtl number $\frac{\mu_f}{\alpha_f (\rho)_f} = \frac{\nu_f}{\alpha_f}$ |
| $Da$ | = | Darcy number = $k/L^2$ |
| $Re$ | = | Reynolds number = $U_0 L/\nu_f$ |
| $Fs$ | = | Forscheimmer number = $b/L$ |
| $Nu$ | = | Nusselt number |

The first author (Dr Ò.À. Bèg) was financially supported by E.P.S.R.C. when the work embodied in this study was originally conducted. It forms part of his PhD thesis in Numerical Hydrodynamics presented to the University of Manchester in March 1996, and both works are fondly dedicated to Mrs Javida K. Bèg. Dr Bèg would also like to express his deepest gratitude to Miss Cathy Dennis, musician and humanitarian, for all the generous help she has provided with his work. Dr Bèg also takes great pleasure in personally thanking all the nursing staff at Withington Hospital, Cavendish Road, Manchester, especially Mrs Verena Burgess, Mrs Yoshoda Huckerby, Mrs Karen Bishop and in particular, Miss Sara Rider for their brilliant support during the period May to July 1997 – the final refined work was not acheivable without their tremendous support. Finally a special thankyou to Miss Frances McLoughlin of the Manchester University Schools-Colleges Liaison Service for her kind, gracious attitude to the work.

International Journal of Numerical Methods for Heat & Fluid Flow
Vol. 8 No. 5, 1998, pp. 559–589.

$k$ = permeability of the porous medium
$b$ = Forscheimmer constant
$L$ = standard reference length
$x_0$ = general station along plate

*Greek symbols*
$\alpha$ = Boundary layer parameter $U_0\delta\delta/\nu_f$
$\alpha$ = thermal diffusivity = $\kappa/(\rho C_p)_f$
$\beta$ = coefficient of cubical expansion
$\varepsilon$ = porosity of the medium
$\theta$ = dimensionless temperature variable
$\nu_f$ = fluid kinematic viscosity $\mu_f/\rho_f$
$\kappa$ = stagnant thermal conductivity of fluid-saturated porous medium
$\kappa_f$ = fluid thermal conductivity
$\lambda$ = thermal conductivity ratio $\kappa_f/\kappa$
$\mu_f$ = fluid dynamic viscosity
$\mu'$ = effective viscosity of medium (Brinkman-modified viscosity)
$\Lambda$ = fluid-matrix viscosity ratio = $\mu'/\mu_f$
$\delta$ = boundary layer thickness $\left[\frac{2\alpha(x_{x_0})\nu_f}{U_o}\right]^{1/2}$
$\eta$ = spanwise pseudo-similarity coordinate
$\xi$ = streamwise pseudo-similarity coordinate
$\rho_f$ = fluid density
$\psi$ = stream function

*Superscripts*
$'$ = differentiation with respect to $\eta$.
$\cdot$ = differentiation with respect to x

*Subscripts*
$f$ = fluid
$w$ = wall condition
$\infty$ = free stream condition

*Abbreviations*
LHS left hand side
RHS right hand side

## Introduction

The analysis of free and forced convection heat transfer in fluid-saturated porous media finds applications in a tremendously wide range of environmental and industrial fields including groundwater pollution[1], energy storage in aquifers[2], biophysical heat transfer[3], subterranean deposition of heat-generating materials[4], volcanic and geophysical flows[5] etc. In petroleum reservoir engineering[6] the understanding of porous convection is of great significance, since this comprises the basic mode of oil and gas circulation via rocks and sandstone, enhanced oil recovery methods, oil shale harvesting, and *in situ* reservoir combustion techniques[6]. To exploit geothermal energy effectively and successfully, engineers require a knowledge of initiating convection currents in geothermal fluids[7,8]. Convective flow in particular is also observed frequently during filtering and drying processes[9] and in packed-bed chromatography. In electronic engineering, cooling mechanisms for semi-conductor devices have been modified by the introduction of porous wafer layers. In solar energy systems “porous” absorbers have proved revolutionary in optimising the storage of absorbed solar energy. Thermal losses from the receiver of a concentrating solar collector often dominate the performance of the collector system under high temperature operations. Conventional line focus receiver designs incorporate transparent enclosures and selective surfaces to minimize convective and radiative heat transfer losses. Many innovative designs have been proposed and implemented in practice, exploiting the property of porosity, and have operated with lower losses at elevated temperatures compared with original designs, with the added advantage of ease of construction and inexpensiveness of materials, as discussed at length by Duffie and Beckman[10].

The vast majority of studies of convection in porous media have employed the classical Darcy formulation introduced over a century ago and later re-formulated by Dupuit[11] as the macroscopic equation of motion for Newtonian fluids in porous media at a low Reynolds numbers range of 1-10, who showed the flow to be linearly dependent upon the pressure gradient and the gravitational force. The mean filter velocity (seepage velocity or Darcy velocity) **v** was taken to be proportional to the sum of the pressure gradient $\nabla p$ and the gravitational force gradient $\nabla \mathbf{g}$, but the important effect of "inertia" was neglected, leading to the modern form of the Darcy equation viz:

$$v = \frac{constant}{\mu}(\nabla p + \rho g) \tag{1}$$

This century a number of modelling techniques for porous media hydrodynamics have been developed,which implement various different mathematical theories such as random fields, homogenisation theory, spectral analysis or geometrical structures. These models are more concerned with the structure of the porous medium and its local and global properties as opposed to the bulk effects of the medium on flow or heat transfer. These latter considerations, being of paramount importance in engineering fluid mechanics, have led to a preference for mathematical models which translate porosity effects into an "additional resistance term" added to the standard flow equations, such as the Navier Stokes equations or more popularly the boundary layer equations – these constitute drag force models. Clearly the most basic drag force type model is the Darcy flow model – unfortunately this yields minimum information about the properties of the permeability of the porous medium and cannot simulate any boundary friction effects which are vital in the accurate modelling of viscous fluid flows. Darcy's law simulates only bulk resistance, and therefore the Dutch petroleum engineer Brinkman[12] re-assessed the problem of flow in porous media to capture the effect of viscous diffusion or boundary friction, this investigation culminating in the so-called Brinkman equation, which is fundamentally a "viscous force" equation, as described by Bear and Bachmat[13]. Brinkman produced a relationship for the porosity $\varphi$ of "an assemblage of spherical particles" and the permeability $k$. He assumed that porosity $\varphi$ was of sufficient magnitude to validate his equation for incompressible flow past an individual sphere i.e. $\nabla^2 \mathbf{v} = 0$ and basically superimposed the viscous penetration dominated flow (Stokes creeping flow) with the Darcy flow. This fundamental work was, as discussed by Nield[14], more than simply an extension of the Darcy law. It does not include inertial effects but instead incorporates an extra Laplacian type viscous term $\mu \nabla^2 \mathbf{v}$. Consequently the Brinkman equation, which is a heuristic momentum equation, states, in the absence of a body force:

$$\nabla p = \left(\frac{\mu}{k}\right) v + \mu' \nabla^2 v \tag{2}$$

where $\mu$ denotes the Newtonian dynamic viscosity. Initially in his study Brinkman used the Einstein formulation for the effective viscosity of a suspension,viz:

$$\mu' = \mu[1 + 2.5(1 - \varepsilon)] \quad (3)$$

The last term in (2) is commonly called the Brinkman term and it is analogous to the "diffusion term" in the Navier-Stokes equations or macroscopic bulk viscous shear-stress diffusion. Nield and Bejan[15] have indicated that this extension was carried out to account for the transition from Darcy flow to highly viscous flow (in the absence of a porous medium) in the limit of extremely high permeability i.e. approaching the situation of a pure fluid or "clear" flow. It is now well understood that the effects of a solid boundary on flow in a porous medium originate from the momentum diffusion generated by the boundary frictional resistance or "Brinkman friction" which accompanies the bulk frictional drag (Darcy resistance which is induced by the solid matrix).

Experimentally, Lundgren[16] has shown that the Brinkman model is valid only at very high porosity values i.e. nearing unity. A figure of 0.95 has been suggested by Durlofsky and Brady[17].The utility of the Brinkman equation formulation is therefore demonstrated by problems in which the permeability is high near the boundary i.e. the particles are "loosely" packed so that there exists a boundary layer thickness in close proximity to the surface. The boundary layer at the wall has been experimentally proven by Beavers and Joseph[18] to be very thin – of the order of several particle diameters, and there is a discrepancy between the effective and bulk viscosity, the former varying within the boundary layer. The Brinkman results for permeability have shown some digression from experimental results. To overcome these discrepancies many investigators have suggested modifications of the Brinkman equation. There is a discrepancy between the Brinkman theory and experiment when normal fluid viscosity is used for the matrix-fluid combination, the effective viscosity $\mu'$ concept overcomes this. $\mu'$, which is a bulk property, is a function of both the structural properties of the matrix and the fluid viscosity. In Lundgren's major work[16], a justification of the Brinkman equation is provided and it is demonstrated that the ratio of $\mu'$ to the fluid viscosity $\mu$ is not always greater than 1. Lundgren's analysis is for dilute concentrations of spheres and it has been suggested that the decrease in the effective viscosity for larger concentrations is caused by the diluteness. The analysis basically involves non-uniform flow via a dilute bed of spheres. The mean transition or drag at a point is determined by Lundgren[16] and then finally the $\mu'$ coefficient calculated using the Brinkman equation.

The Brinkman model is frequently used in the analysis of heat and fluid flow in "composite" media or porous-plain media. As discussed above, several modifications have been made to the Darcy law, e.g. the addition of a macroscopic shear term to the Darcy equation (with $\mu' = \mu$) to simulate velocity variations near the boundary, or e.g. the rigorous validation of the Brinkman

extension to the Darcy formulation, for dilute concentrations of particles. Kaviany[19] has shown that the interface velocity obtained from the Brinkman equation is the same as that obtained from the "local" simulation, within a minute margin of error, by comparing the one-D Brinkman model with "direct simulation" or volume-averaged point solution.

Prasad and Kladias[20] have emphasized that whilst the "viscous drag effect" may be of relative insignificance for isothermal boundary layer flows, nevertheless, owing to the association of convective heat transfer with boundary layer phenomena, the viscous effects, i.e. vorticity diffusion, have a great influence on the convective transport of energy. Owing to the presence of the macroscopic shear term the Brinkman equation exhibits full compatibility with boundary layer regions within porous media. Nield and Bejan[15] have discussed the validity of including the Brinkman term in many studies, particularly for models involving both Forscheimmer inertial effects and Brinkman boundary effects – the Forscheimmer model works best at low porosities in contrast to the Brinkman model which is really only valid at larger porosities. The question immediately arises as to whether either approximation is valid at the opposite extremity. A compromise may be to use intermediate porosities such as 0.4-0.7 which typify geothermal reservoirs.

Evans and Plumb[21] examined theoretically the boundary layer flow past a vertical isothermal surface, indicating that for Darcy numbers $Da < 10^{-7}$ ( Da being defined by $k/L^2$, k the permeability, $L$ being the plate length), the viscous boundary effect was not significant. A lower rate of heat transfer was predicted with the Brinkman term included. Ganapathy and Purushothaman[22] studied thermal convective flow from an instantaneous point source in a porous domain. They concluded that the boundary friction decelerated the momentum transfer at all times and exerted an influence at radial distances up to order $K^{1/2}$ from the source. Sen[23] considered the Darcy-Brinkman convective flow in a shallow porous layer with adiabatic upper and lower plate boundaries and constant-temperature lateral boundaries, noting a transition in the effect of the viscous boundary effect on the Nusselt number only above Darcy numbers of 0.0001 after which the Nusselt number was seen to plummet, due to a decrease in velocity in close proximity to the wall.

Boundary layer studies were also performed by Vasseur and Robillard[24], Tong and Subramanian[25], Tong and Orangi[26] on free convection in vertical enclosures, i.e. cavities with various aspects ratios. Invariably it was observed that as the Brinkman effect rose the heat transfer rate fell again owing to the velocity decrease at the wall. Takhar *et al.*[27] recently studied the mixed convective flow past a hot vertical plate in a porous medium using a permeability parameter and a porous Reynolds number. Numerical non-similar asymptotic solutions were sought using a fourth-order Runge-Kutta scheme. An increase in skin-friction was shown to accompany a rise in permeability.

The boundary layer flow in an annulus was studied by Parang and Keyhani[28], heat flux being imposed on both cylinder walls. The Brinkman term was shown to be only significant for values of $Da/\phi. > 10^{-5}$, ($\phi$ denoting

porosity) these being most severe at the external wall, the rate of heat transfer falling here, accompanied by a rise in temperature.

The present study is aimed at collectively studying the combined effects of bulk first order porous matrix resistance (Darcy effect), boundary friction (Brinkman effect), frictional work (viscous dissipation) and thermal conductivity ratio ($\lambda$) on the boundary layer heat transfer past a vertical heated plate in a fully-saturated porous regime. Such a study may be regarded as an extension of the previous study by Takhar *et al.*[27] to include the supplementary effect of various thermal conductivity values for the porous medium, with an alternative momentum equation formulation, and has not been studied in the literature. Additionally we have obtained solutions with both Keller's finite difference scheme and the shooting scheme (DSRK), the earlier study[27], however, employing only the shooting method.

**Mathematical model**

Consider the steady two-dimensional mixed convective boundary layer flow of a Boussinesq fluid along a hot flat vertical plate embedded in a homogeneous, isotropic non-Darcian porous medium. With reference to a Cartesian coordinate system ($x,y$) with $x$-axis directed parallel to the plate and flow direction and $y$-axis normal to the plate, the governing equations may be expressed in the form:

$$\frac{\partial u}{\partial x} + \frac{\partial v}{\partial y} = 0 \tag{4}$$

$$\frac{\rho_f}{\varepsilon^2}\left[u\frac{\partial u}{\partial x} + v\frac{\partial u}{\partial y}\right] = \frac{\mu_f . u}{k} + \rho_f g\beta(T\ T\infty) + \frac{\mu'}{\varepsilon}\frac{\partial^2 u}{\partial y^2} \tag{5}$$

$$\rho Cp[u\frac{\partial T}{\partial x} + v\frac{\partial T}{\partial y}] = \kappa\frac{\partial^2 T}{\partial y^2} + \mu_f\left(\frac{\partial u}{\partial y}\right)^2 \tag{6}$$

with corresponding boundary conditions :

$$u(x,0) = 0,\ v(x,0) = 0,\ T(x,0) = T_W$$
$$u(x,\infty) = U_\infty,\ T(x,\infty) = T_\infty \tag{7}$$

The following important assumptions are made:

(1) The effects of inertia (Forscheimmer second order drag), hydrodynamic and thermal dispersion are ignored.

(2) Thermophysical properties of the solid and the fluid are constant except for the buoyancy term.

(3) Local thermal equilibrium is assumed between the solid matrix particles and the percolating fluid allowing a continuum treatment.

(4) The porous medium is assumed to be rigid, i.e. non-deformable, homogeneous and isotropic with all void-spaces connected.

The appropriate transformed boundary layer equations in dimensionless form can be shown to take the form:

$$f''' + f''(\alpha f) + 2\alpha\xi \frac{\partial f}{\partial \xi}(f') - 2\alpha\xi \frac{\partial^2 f}{\partial \xi \partial \eta}(f') + 2\alpha\xi(\theta) - 2\alpha\xi\left(\frac{Re}{GrDa}\right) f' = 0 \quad (8)$$

$$\left(\frac{1}{Pr}\right)\theta'' + \lambda E_c (f'')^2 + \lambda(\alpha f)\theta' + 2\alpha\lambda\xi\theta' \frac{\partial f}{\partial \xi} - 2\alpha\lambda\xi f' \frac{\partial \theta}{\partial \xi} = 0 \quad (9)$$

where

$$\eta = \frac{y}{\delta(x)}, \xi = g\beta\Delta T(x-x_0)\varepsilon^2/U_0^2L^2, \psi = U_o\,\delta(x).f(\xi,\eta),$$

$$u = \frac{\partial \psi}{\partial y}, v = \frac{\partial \psi}{\partial x}, \delta(x) = \left[\frac{2.\alpha.(x-x_o).\nu_f}{U_o}\right]^{1/2}, \alpha = U_0\,\delta\delta^{\circ}/\nu_f \quad (10)$$

$$\theta = (T - T_\infty)/(T_W - T_\infty) = (T - T_\infty)/(\Delta T).$$

The appropriate pseudo-similarity boundary conditions are :

$$f(\xi,0) = 0 \qquad f'(\xi,0) = 0, \quad \theta(\xi,0) = 1$$
$$f'(\xi,\infty) = 1, \quad \theta(\xi,\infty) = 0 \quad (11)$$

**Computational solution by Keller-box implicit scheme**

The similarity equations (8) and (9) are to be solved with an implicit central finite differencing scheme employing Newton's quasi-linearization and block tridiagonal elimination described at length by Cebeci and Bradshaw[29]. Originally developed for both laminar and turbulent aerodynamic boundary layer flows at the California Institute of Technology in 1970, by Professor Herbert B. Keller[30], this is a finite-difference scheme which has proven to be

extremely successful in solving parabolic systems. Keller's method is implicit, which implies that the unknown variable at the "downstream" station is expressed in terms of its juxtaposed values immediately downstream and the known quantities. Implicit methods can determine all the flow variables perpendicular to the principal stepping direction (e.g. $\xi$ simultaneously).

Keller's scheme demonstrates greater speed, swifter compilation and superior adaptability to the majority of other numerical methods used for boundary layer flows. The Keller-Box scheme, which is implicit, exhibits optimisation of a number of highly desirable features which supersede the limitations of the vast majority of boundary-layer numerical solvers, and therefore greatly ameliorates the solution of general parabolic non-linear PDEs. These are :

(1) Ability to solve systems of differential equations of any order and therefore not only second order as typified by the laminary steady thin shear layer, i.e. boundary layer equations which are used when heat and momentum transfer rates are presumed to depend only on diffusivities. This means that heat, momentum and mass transfer (species concentration) similar boundary layer flows can be solved which usually have a total order of seven and also angular momentum flows (additional 2nd order PDE). Very high order equations can be accommodated with minimal digital computing – the only drawback is the marked increase in algebraic mathematics with rising order for the derivation of the matrix solver subroutine SOLV5[29].

(2) Second order accuracy can be realised with arbitrary non-uniform spacing in two-dimensions ($x,y$). Finite difference equations are generated with a truncation of order $O\,(\Delta\eta^2)$ i.e. errors of order $O\,(\Delta\eta^2)$. Cebeci and Bradshaw[29] emphasize that the objective of "accuracy" in boundary layer computations is to obtain solutions using comparatively few mesh points rather than high-digit output. Lesser mesh points lead to faster iteration convergence and therefore higher programming efficiency. Keller's method demonstrates this feature very effectively.

(3) Keller's scheme allows very rapid $x$ or $\xi$ (streamwise similarity variable) variation which is vital for turbulent boundary layer computations or complex flows with supplementary effects such as magnetism, radiation, vortex instability etc.

(4) Keller's approach facilitates the programming of a large number of coupled equations directly suiting heat and mass transfer problems.

(5) Keller's method employs the approach of quickly transforming high order equations to the form of a multiple first-order system. In the boundary layer equations the derivatives of certain quantities w.r.t. the spanwise or normal variable $\eta$, e.g. $\partial^2 u/\partial\eta^2$ must, by necessity, be introduced as the new unknown functions. Fortunately, owing to the power of the boundary layer theory approximation derivatives, w.r.t. all other streamwise variables appear only to first order. The standard

Keller box steps are applied to each ODE in turn leading to Keller "momentum" and "energy" coefficients. Initially the governing equations are transformed from the real $x,y$ coordinates to the pseudo-similarity coordinates $\xi$ and $\eta$ so that the boundary layer thickness in $(\xi,\eta)$ coordinates is nearly independent of the streamwise distance and can therefore be represented by a fixed number of profile points at fixed spacing. The scheme is executed in four distinct stages:

(1) Reduction of the high order ODEs to a multiple system of first order ODEs.

(2) Finite-difference formulation of the ODEs in terms of central Newtonian finite-difference operators. Effectively a "grid" or finite-difference "mesh" is superimposed on the flow field and this defines the solution domain. The flow variables are computed at only the intersection points or "nodes" of the grid. Systematically, therefore, algebraic equations are generated for each mesh point from the PDEs with the relevant boundary conditions which must exactly equal the number of unknown variables to ensure the "well-posedness" of the problem. Grid size is crucial with respect to the desired accuracy of a computation and is intricately associated with numerical stability.

(3) Linearization of the resulting non-linear algebraic equations and conversion into a matrix-vector system.

(4) Block tridiagonal elimination solution of the linearised matrix-vector system using an improved algorithm.

Initially the boundary layer similarity equations are reduced to a set of five first order equations by introducing new unknown functions of $\eta$-derivatives:

$$f' = U \tag{12a}$$

$$U' = V \tag{12b}$$

$$(V)' + \alpha fV + 2\alpha\ \xi\theta\ \ 2\alpha\left(\frac{Re}{GrDa}\right)\xi\ U = 2a\xi\left[U\frac{\partial U}{\partial \xi}\ \ V\frac{\partial f}{\partial \xi}\right] \tag{12c}$$

$$\theta' = G \tag{12d}$$

$$\left(\frac{1}{Pr\lambda}\right)(G)' + Ec\,(V)^2 + \alpha fG = 2\alpha\xi\left[U\frac{\partial \theta}{\partial \xi}\ \ G\frac{\partial f}{\partial \xi}\right] \tag{12e}$$

and the boundary conditions become :

$$f(\xi,0) = 0, \qquad U(\xi,0) = 0, \quad \theta(\xi,0) = 1$$
$$U(\xi,\infty) = 1, \quad \theta(\xi,\infty) = 0. \tag{13}$$

A two-dimensional net is now superimposed on the $\xi$-$\eta$ plane defined by:

$$\xi_0 = 0; \ \xi_n = \xi_{n-1} + k_n, \ n = 1,2,3,4...N.$$
$$\eta_0 = 0; \ \eta_j = \eta_{j-1} + h_j, \ j = 1,2,3,4,....J \tag{14}$$

Approximating the quantities $f, U, V, \theta, G$ at the points $\xi^n, \eta_j$ on the net by $f_j^n, U_j^n, V_j^n, \theta_j^n, G_j^n$ then the following non-linear algebraic equations are obtained:

$$h_j^{-1}[f_j'' - f_{j-1}''] = U_{j-1/2}''$$

$$h_j^{-1}[U_j'' - U_{j-1}''] = V_{j-1/2}''$$

$$h_j^{-1}[\theta_j'' - \theta_{j-1}''] = G_{j-1/2}''$$

$$h_j^{-1}[V_j'' - V_{j-1}''] + C_1 [fV]''_{j-1/2} - C_3 (\xi^{n-1/2}) [U''_{j-1/2}] + C_2 (\xi^{n-1/2}) [\theta''_{j-1/2}]$$

$$- C_2(\xi^{n-1/2}/k_n) \{[(U^2)]''_{j-1/2} - [V''_{j-1/2} f''_{j-1/2} - V''_{j-1/2} f''^{n-1}_{j-1/2} + V''^{n-1}_{j-1/2} f''_{j-1/2}]\} = R^{n-1}_{j-1/2}$$

$$C_4 h_j^{-1}[(e_j'' G_j'' - e_{j-1}'' G_{j-1}'')] + (C_1)[fG]''_{j-1/2} + (C_5)[V^2]''_{j-1/2}$$

$$- (C_2)(\xi^{n-1/2}/k_n)[\{(U\theta)''_{j-1/2} - U''_{j-1/2} \theta^{n-1}_{j-1/2} + U^{n-1}_{j-1/2} \theta''_{j-1/2}\} \tag{15a-e}$$

$$-\{(fG)''_{j-1/2} - G''_{j-1/2} f^{n-1}_{j-1/2} + G^{n-1}_{j-1/2} f''_{j-1/2}\}] = T^{n-1}_{j-1/2}$$

where $h_j$ denotes the $\eta$ step distance and $k_n$ designates the $\xi$ step length and where:

$$C_1 = \alpha, C_2 = 2\alpha, \ C_3 = 2\alpha(Re/GrDa), C_4 = 1/\lambda Pr, \ C_5 = Ec.$$

$$R^{n-1}_{j-1/2} = -h_j^{-1}[V_j^{n-1} - V_{j-1}^{n-1}] - C_1 [fV]^{n-1}_{j-1/2} + C_3 (\xi^{n-1/2})[U^{n-1}_{j-1/2}] - C_2 (\xi^{n-1/2})[\theta^{n-1}_{j-1/2}]$$

$$- C_2 (\xi^{n-1/2}/k_n)[(U^2)^{n-1}_{j-1/2} - (V^{n-1}_{j-1/2} f^{n-1}_{j-1/2})]$$

$$T^{n-1}_{j-1/2} = -C_4 h_j^{-1}[e_j^{n-1} G_j^{n-1} - e_{j-1}^{n-1} G_{j-1}^{n-1}] \tag{16}$$

$$- C_1 [fG]^{n-1}_{j-1/2} - (C_5)[V^2]^{n-1}_{j-1/2} + C_2 (\xi^{n-1/2}/k_n)[(fG)^{n-1}_{j-1/2} - (U0)^{n-1}_{j-1/2}]$$

The non-linear algebraic equations (15a-e) are now solved using Newton's quasilinearisation method for which the iterates $f_0^{(i)}, U_0^{(i)}, V_0^{(i)}, \theta_0^{(i)}, G_0^{(i)}$ are introduced valid for $i = 0,1,2,3,4 \ldots J$ with initial values equal to those at the previous $\xi$-station (this generally being the most bankable guess available). For the higher order iterates we set:

$$f_j^{(i+1)} = f_j^{(i)} + \delta f_j^{(i)}, \quad U_j^{(i+1)} = U_j^{(i)} + \delta U_j^{(i)},$$
$$V_j^{(i+1)} = V_j^{(i)} + \delta V_j^{(i)}, \quad \theta_j^{(i+1)} = \theta_j^{(i)} + \delta \theta_j^{(i)}, \tag{17}$$
$$G_j^{(i+1)} = G_j^{(i)} + \delta G_j^{(i)},$$

where $\delta$ denotes the "error" in the estimate. Substitution of the RHS of these expressions with the subsequent omission of quadratic terms in $\delta f_j^{(i)}$, $\delta U_j^{(i)}$, $\delta V_j^{(i)}$, $\delta \theta_j^{(i)}$, $\delta G_j^{(i)}$ generates the Keller "linearized" difference equations with corresponding finalized boundary conditions. The resulting linearized algebraic equations, which we do not state for conciseness, are solved numerically under the appropriate boundary conditions using an extremely efficient and computationally robust block-factorization technique[30] which has been applied successfully by a number of researchers including Gorla[31] and Beg *et al.*[32]. The system of linearized finite-difference equations is eventually rewritten in the linear matrix-vector form :

$$A\ \delta_j = r_j \tag{18}$$

where **A** designates the " Keller coefficient matrix" of rank $5 \times 5$ (for 5th order systems) which is discussed below and $\delta_j$ and $\mathbf{r_j}$ denote the fifth order vectors for the perturbation quantities and RHS residuals in the linearised equations. In writing the linearized system a specific pattern is maintained. This is performed in order to ensure non-singularity of the sub-hierarchical matrix $A_0$ in **A**, which guarantees that the square matrix $A_0$ has an inverse $A_0^{-1}$ and this inverse is unique ($A_0 . A_0^{-1} = A_0^{-1} . A_0 = I$). The resulting system is a fifth order linear system ($f^{///}, \theta^{//}$). Owing to its block-tridiagonal structure, the system can be implemented very successfully. The solution procedure is inherently very rigorous algebraically and to facilitate the mathematics, it is cast into matrix-vector form. The block elimination technique is a general method and can be employed for any number of first-order equations, although as the order of the system increases, extremely voluminous algebra becomes unavoidable in tackling the "recursion" formulae which are generated, although for a fifth order system, the amount of hand-analysis is manageable. We first define the fifth-dimensional vectors:

$$r_j = [\ (r_1)_j\ \ (r_2)_j\ (r3)_j\ \ r_4)_j\ \ (r_5)_j\ ]^T$$
$$\delta_j = [\ (\delta f_j)\ \ (\delta u_j)\ (\delta v_j)\ \ (\delta g_j)\ \ (\delta p_j)\ ]^T \tag{19}$$

where $\mathbf{r_j}$ designates the RHS of the finite difference equations, and $\Delta_j$ denotes the vector of errors, i.e iterates, and T denotes transpose. In terms of these vectors the finite difference equations for both the momentum and energy equations can be formulated as:

$$R_j \delta_j - L_j \delta_{j-1} = r_j \qquad j = 1,2,3 \ldots J \tag{20}$$

where $\mathbf{R_j}$ and $\mathbf{L_j}$ are coefficient matrices of order $5 \times 5$, and $\delta_{j-1}$ denotes the iterate vector at the previous step. The finite difference equations have to be rearranged in order to comply with the order of the "$\delta_j$" vectors and the $r_j$ vector. The complete linear system of equations (20) can be shown to be cast as the block matrix system or in compound block matrix notation, we can cast the above system as:

$$A.\delta = r \tag{21}$$

where **A** is as the matrix of coefficients. It can be inferred that the non-zero elements in the coefficient matrix are clustered about the diagonal. Thus various "band-matrix" procedures can be adopted to solve the system of $\mathbf{A}\delta = \mathbf{r}$. Keller implements the following tridiagonal factorization scheme which demonstrates superior efficiency to the conventional band-matrix routines. The coefficient matrix is of order $5J + 5$, and the vectors $\delta$ and **r** also have this dimension. We therefore decompose **A** into $5 \times 5$ blocks starting from the upper-left-hand corner. Details are provided by Cebeci and Smith[30].Choleski factorization is now employed to simplify the system with the structure $\mathbf{A}\delta = \mathbf{r}$, using the triangularisation principle. The matrix **A** can in this way be orchestrated in the form **A** = **LU**. Proceeding formally using row by column expansion, the following recurrence relations can be deduced:

$$\begin{aligned} \Delta_0 &= A_0 \\ \Gamma_j . \Delta_{j-1} &= B_j \\ \Delta_j &= A_j - \Gamma_j C_{j-1} \qquad j = 1,2 \ldots .J \end{aligned} \tag{22}$$

Keller[33] has shown with rigorous mathematical detail that the $\Gamma_j$ matrix has the same structure as that of the the $\mathbf{B_j}$ matrix. The $\Delta_j$ matrix also has a similar structure to $\mathbf{A_j}$. The $\Delta_j$ matrix "elements" are calculated using the recurrence relation:

$$\Delta_j = A_j - \Gamma_j C_{j-1} \qquad 1 \le j \le J. \tag{23}$$

The elements of the $\Gamma_j$ matrix are generated by implementing the recurrence relation,

$$\Gamma_j \Delta_{j-1} = B_j \tag{24}$$

Cebeci and Bradshaw[29] rewrite equation $\mathbf{A}.\delta = \mathbf{r}$, using now the **L.U** factorisation method, viz:

$$L.U.\delta = r \tag{25}$$

where they set;

$$U.\delta = w \tag{26}$$

so that (25) becomes:

$$L.w = r \tag{27}$$

Consequently, from the recurrence relations the double sweep operation is executed, viz forward and backward sweeps to compute the $\delta$ components. Following the block elimination computations the initial profiles for functions $f,U,V,\ \theta,G$ are generated and then used to march along the boundary layer in the streamwise direction solving for $\xi$.

**Numerical shooting computations**

The momentum and energy equations (8) and (9) are now solved by a shooting technique described comprehensively by Bèg[33] and Gorla and Takhar[34]. We expand $f$ and $\theta$ in powers of the streamwise coordinate $\xi$ as follows, this procedure being valid for $\xi < 1$:

$$f(\xi,\eta) = f_0(\eta) + \xi f_1(\eta) + \xi^2 f_2(\eta) + \ldots$$
$$\theta(\xi,\eta) = \theta_0(\eta) + \xi\theta_1(\eta) + \xi^2\theta_2(\eta) + \ldots \tag{28}$$

Denoting $\Phi$ = Re/GrDa, differentiating the expansions with respect to the similarity coordinates $\xi$ and $\eta$, truncating at second order and substituting into the momentum equation and energy equation yields the following set of six ordinary differential equations which govern the velocity (momentum) and temperature field:

$$f_0''' + (\alpha f_0)f_0'' = 0$$
$$f_1''' + (\alpha f_0)f_1'' + 3\alpha f_0''f_1 - 2\alpha f_0' f_1' + 2\alpha\theta_0 - 2\alpha\Phi f_0' = 0 \tag{29a-c}$$
$$f_2''' + 5\alpha f_2 f_0'' + 3\alpha f_1''f_1 + (\alpha f_0)f_2'' - 4\alpha f_0' f_2' - 2\alpha f_1' f_1' + 2\alpha\theta_1 - 2\alpha\Phi f_1' = 0$$

$$\theta_0'' + Pr\lambda[\alpha f_0]\theta_0' + Pr\lambda Ec[(f_0'')^2] = 0$$
$$\theta_1'' + Pr\lambda Ec[2f_0''f_1''] + 2\alpha Pr\lambda(f_1\theta_0') + Pr\lambda\{(\alpha f_0)\theta_1' + \alpha f_1\theta_0'\} - 2\alpha Pr\lambda[f_0\theta_1] = 0 \tag{30a-c}$$
$$\theta_2'' + Pr\lambda Ec[2f_0''f_2'' + (f_1'')^2] + Pr\lambda[(\alpha f_0)\theta_2'] + Pr\lambda[\alpha f_1\theta_1' + \alpha f_2\theta_0'] + 2\alpha Pr\lambda[2\theta_0' f_2 + \theta_1' f_1] - 2\alpha Pr\lambda[2f_0'\theta_2 + f_1'\theta_1] = 0$$

Although the power series expansions are convergent for $\xi < 1$, they can be generalised to converge for $\xi < 1$ using non-linear transformation techniques developed by Shanks for divergent or slowly-convergent series[33].The system of ODEs (29 a-c), (30a-c) can now be numerically integrated using fourth-order

Runge-Kutta-Merson quadrature supplied by the powerful **NAG** library routines. This method is an extension of the conventional Runge-Kutta shooting scheme (which marches unidirectionally, say from zero to infinity) for the case of two point boundary value problems. The double-shooting scheme therefore in addition has to shoot back from infinity to zero, a process which is repeated until a certain convergence criterion has been satisfied. In the DSRK scheme both initial and boundary values are given and the multiple order equations generated by the Taylor expansions are solved by integration of these ordinary differential equations with Runge-Kutta-Merson stepping formulae, embodied in the **NAG** routine **DO2HBF.** The range of integration is split into equal increments ($\Delta x$ where $x = \eta$) and the computation progresses from $x = 0$ (initial condition) in successive increments to the final boundary condition. Systematically, therefore, for a set of ordinary differental equations given by:

$$dQ_i/dx = f_i(x, Q_1, Q_2, Q_3, Q_4, \ldots\ldots\ldots\ldots, Q_n) \tag{31}$$

the solution is advanced from xn to $x_n + H = x_{n+1}$, the integration step being designated by $H$. The value of the general function $Q$ is given by the formula:

$$Q_{n+1} = Q(x_n + H) = Q_n + H/6\,[Z_1 + 4Z_4 + Z_5]$$

where

$$\begin{aligned}
Z_1 &= f[x_n, Q_1, Q_2, \ldots\ldots, Q_n] \\
Z_2 &= f[x_n + H/3, Q_1 + Z_1/3, Q_2 + Z_1/3, Q_3 + Z_1/3, \ldots, Q_n + Z_1/3] \\
Z_3 &= f[x_n + H/3, Q_1 + (Z_1 + Z_2)/6, Q_2 + (Z_1 + Z_2)/6, Q_3 + (Z_1 + Z_2)/6 \\
&\qquad \ldots\ldots\ldots, Q_n + (Z_1 + Z_2)/6] \\
Z_4 &= f[x_n + H/2, Q_1 + (Z_1 + 3Z_3)/8, Q_2 + (Z_1 + 3Z_3)/8, \\
&\quad Q_3 + (Z_1 + 3Z_3)/8, \ldots\ldots\ldots, Q_n + (Z_1 + 3Z_3)/8] \\
Z_5 &= f[x_n + H, Q_1 + (Z_1 - 3Z_3 + 4Z_4)/2, Q_2 + (Z_1 - 3Z_3 + 4Z_4)/2, \\
&\quad Q_3 + (Z_1 - 3Z_3 + 4Z_4)/2, \ldots\ldots\ldots, Q_n + (Z_1 - 3Z_3 + 4Z_4)/2]
\end{aligned} \tag{32}$$

The higher the order, the greater the diversity of possible schemes in the extended Runge-Kutta method, and the lower the truncation error. The NAG routine **DO2HBF** is extremely large and in fact composed of over 30 smaller subroutines which each perform a specific numerical task. Details are provided by Beg[34]. Here we briefly mention the important routine **DO2SAF** which is responsible for computing the Jacobian matrix whose $(i,j)$th element depends on the derivative of the general function $Q_i$ with respect to the $j$th boundary condition parameter denoted P(J) in the program. The matrix is evaluated by a numerical differentaiation technique requiring $N1$ integrations of the multiple first order system (29a-c), (30a-c), where $N1$ designates the quantity of

unspecified boundary conditions. Owing to the sensitivity of numerical stability to the mesh step size, a mediocre and well-tested value of 0.1 in the $\eta$ direction was used and typical compilation times averaged around 300 seconds on a 66 MHz VICTOR Computer.

**Results and discussion**

The surface shear stress, i.e. local skin friction function $C_f / 2(Re_x)^{1/2}$ and local heat transfer parameter i.e. local Nusselt number function $Nu_x/(Re_x)^{1/2}$ are defined by:

$$C_f / 2(Re_x)^{1/2} = f''(\xi,0)$$
$$- Nu_x/(Re_x)^{1/2} = \theta'(\xi,0) \qquad (33a,b)$$

Figures 1a,b to 2a,b illustrate the surface shear stress $V(\xi,0)$ i.e. $f''(\xi,0)$ and local heat transfer $G(\xi,0)$, i.e. $\theta'(\xi,0)$ profiles (calculated with the Keller-Box method) versus streamwise variable $\xi$ for a number of parameter combinations of $Ec$, $Gr$, $Pr$, $Da$, $Re$ and $\lambda$. Figures 5 to 15a,b show the variation of velocity functions $f_0'(\eta)$, $f_1'(\eta)$, $f_2'(\eta)$ and temperature functions $\theta_0(\eta)$, $\theta_1(\eta)$, $\theta_2(\eta)$ with spanwise coordinate $\eta$ using the Runge-Kutta-Merson double shooting technique (DSRK), results being presented for a number of values of $Ec$, $Gr$, $Pr$, $Da$, $Re$ and $\lambda$ as depicted in the figures overleaf. For the particular case of $\xi = 0.0$ solutions obtained by both Keller-box and DSRK methods are provided.

The effects of the first order porous parameter $Re/GrDa$ where $Da$ is the Darcy number and represents the bulk linear matrix resistance are shown in Figures 4a,b.

Elevation in the Darcy number from 0.002 to 0.05 leads to a large increase in surface shear stress at the wall. An increase in $Da$ causes an increase in the magnitude of local heat transfer parameter $\theta'(\xi,0)$ as depicted in Figure 1b.

The effects of the viscous dissipation parameter – Eckert number $Ec$ – are depicted in Figures 2a,b. Positively increasing $Ec$ values cause a corresponding increase in the shear stress function at the wall and physically $Ec > 0$ corresponds to cooling of the plate (wall). Takhar *et al.*[27] have indicated in their earlier Darcy-Brinkman study that velocity gradients ($f'(\eta)$ etc.) are affected by the enhanced heating of the fluid in the boundary layer leading to an escalation in the "local" velocities in the vicinity of the wall. A more dramatic change in local heat transfer $\theta'(\xi,0)$ is observed [for positive $Ec$ values (0.3,0.5)] which decrease in magnitude. $Ec$ denotes the magnitude of work done by friction. Positive values of $Ec$ correspond to the case of heat extraction, i.e. cooling of the plate surface, as encountered, for example, in fluid withdrawal from geothermal reservoirs and vice versa for negative $Ec$ values. As $Ec$ decreases to –0.3 and –0.5, the shear stress decreases and the plate is heated. The magnitude of the local heat transfer parameter $\theta'(\xi,0)$ is enhanced when $Ec$ becomes negative (plate heating).

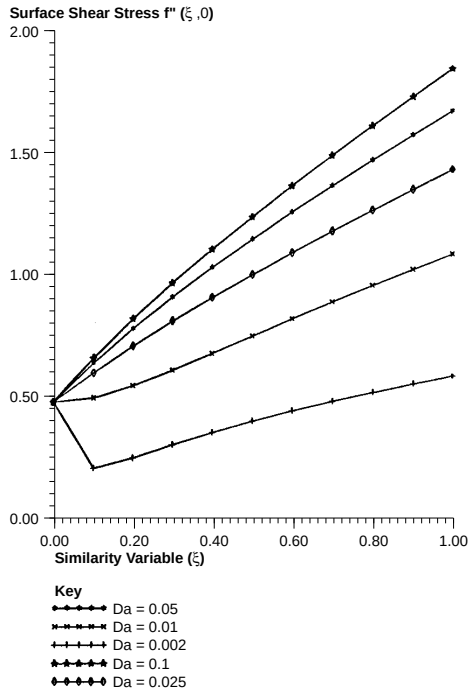


**Figure 1a.**
Variation of $V$ i.e. $f^{//}(\xi,0)$ and $G(\xi,0)$ i.e. $\theta^{/}(\xi,0)$ with streamwise coordinate $\xi$ at the plate surface ($\eta = 0$) for various Darcy ($Da$) numbers; results for Keller box scheme: $\alpha = 1.0$, $Gr = 100$, $Re = 1.0$, $Pr = 0.71$, $Ec = 0.3$, $\lambda = 1.0$

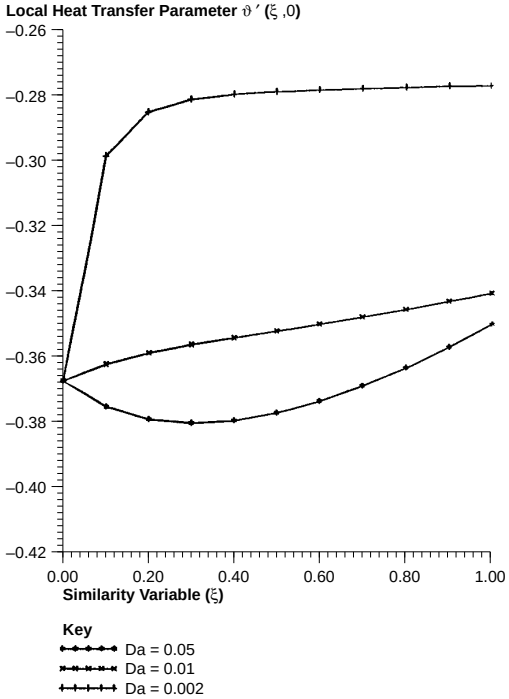


**Figure 1b.**
Variation of $V$ i.e. $f^{//}(\xi,0)$ and $G(\xi,0)$ i.e. $\theta^{/}(\xi,0)$ with streamwise coordinate $\xi$ at the plate surface ($\eta = 0$) for various Darcy ($Da$) numbers; results for Keller box scheme: $\alpha = 1.0$, $Gr = 100$, $Re = 1.0$, $Pr = 0.71$, $Ec = 0.3$, $\lambda = 1.0$

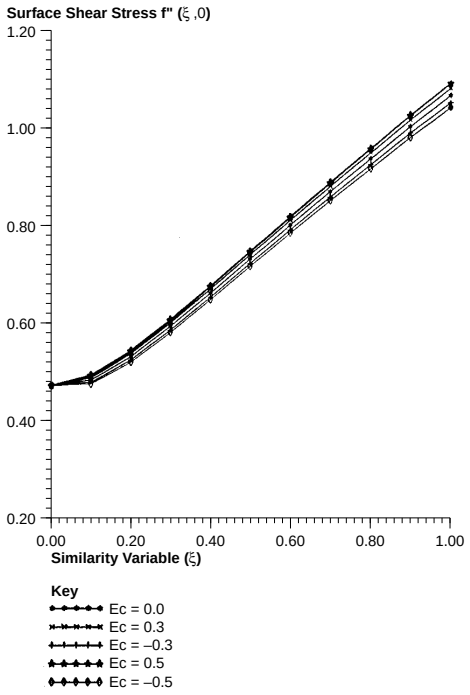


**Figure 2a.**
Variation of $V$ i.e. $f^{/}(\xi,0)$ and $G(\xi,0)$ i.e. $\theta^{/}(\xi,0)$ with streamwise coordinate $\xi$ at the plate surface ($\eta = 0$) for various Eckert numbers ($Ec$); results for Keller box scheme: $\alpha = 1.0$, $Gr = 100$, $Re = 1.0$, $Da = 0.01$, $Pr = 0.71$, $\lambda = 1.0$

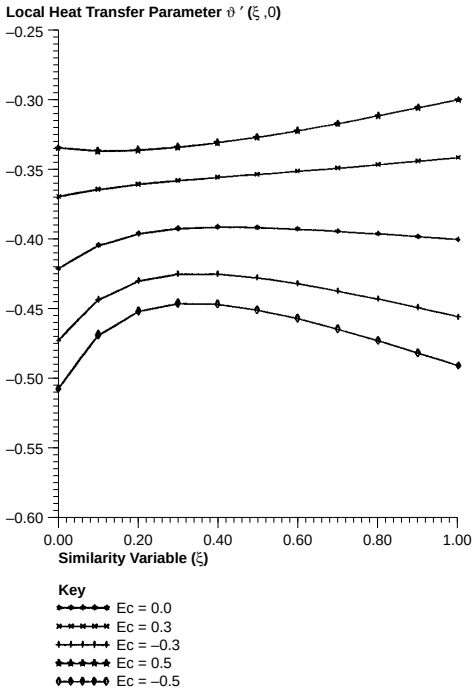


**Figure 2b.**
Variation of $V$ i.e. $f^{/}(\xi,0)$ and $G(\xi,0)$ i.e. $\theta^{/}(\xi,0)$ with streamwise coordinate $\xi$ at the plate surface ($\eta = 0$) for various Eckert numbers ($Ec$); results for Keller box scheme: $\alpha = 1.0$, $Gr = 100$, $Re = 1.0$, $Da = 0.01$, $Pr = 0.71$, $\lambda = 1.0$

The effects of various thermal conductivity ratios $\lambda$ on surface shear stress $V(\xi,0)$, i.e. $f''(\xi,0)$ and local heat transfer $\theta'(\xi,0)$ are given in Figures 3a,b. As $\lambda$ is elevated from a very low value of 0.05 to a mediocre value of 2.0 a distinct reduction in shear stress occurs at the wall. Conversely, local heat transfer magnitudes are dramatically increased with rising $\lambda$ over the same range of $\lambda$ values.

The effects of Prandtl number on surface shear stress $V(\xi,0)$, i.e. $f''(\xi,0)$ and local heat transfer $\theta'(\xi,0)$ can be seen in Figures 4a,b. As $Pr$ is increased from 0.01, which represents liquid metal fluids in e.g. geophysical convective zones and industrial metal flows, through 0.2, 1.0 to 10.0 and 100.0 (corresponding to light and heavy reservoir oils), surface shear stresses are considerably depressed. The magnitude of local heat transfer parameter $G(\xi,0)$ is, however, escalated considerably as $Pr$ rises from 0.01 to 100.

Viscous heating effects (characterized by the Eckert number $Ec$) on temperature functions $f_0'(\eta)$, $f_1'(\eta)$, $f_2'(\eta)$ and $\theta_0(\eta)$, $\theta_1(\eta)$, $\theta_2(\eta)$ can be seen in Figures 5 to 7. A large positive change in $Ec$ has negligible effect on the velocity functions, since the frictional work term does not appear in the momentum equation, and is therefore only very weakly coupled through the temperature equation; therefore velocity plots have been omitted. The dissipative heat effect, however, causes an increase in the magnitude of the temperature function $\theta_0(\eta)$ (Figure 5) from $Ec = 0.0$ (no viscous dissipation) to $Ec = 0.3$, 0.5 (large viscous dissipation and plate cooling). Excellent agreement is observed between the Keller-Box computations performed with $\eta_\infty = 4.0$ and an $\eta$-step distance of 0.1 and the DSRK computed profiles.

Temperatures $\theta_1(\eta)$, $\theta_2(\eta)$ (Figures 6,7) all increase in magnitude consistently as $Ec$ rises from 0.0 through 0.3 to 0.5.

Figures 8a,b-9a,b depict the effects of the porous parameter ($Re/GrDa$) on the velocity and temperature field functions $f_1'$, $f_2'$ and $\theta_1$, $\theta_2$,. A rise in Darcy parameter $Re/GrDa$ from 0.2 to 0.8 causes a decrease in the magnitude of $f_1'$. Temperature function $\theta_1$ decreases markedly in magnitude as ($Re/GrDa$) rises from 0.2 to 0.8. Conversely, the second order velocity function $f_2'$ increases substantially positively although values are generally negative. The second order temperature function $\theta_2$ on the other hand is diminished with rising ($Re/GrDa$) parameter since this implies decreasing Darcy number $Da$ which physically translates as a lower permeability of the porous matrix for any stipulated $Re$ and $Gr$ values, i.e. less space for the fluid to move through implying reduced convection heat transfer, and enhanced conduction.

The profiles for velocity functions $f_1'$, $f_2'$ and temperature functions $\theta_0$, $\theta_1$, $\theta_2$,versus $\eta$ for various $\lambda$ values are illustrated in Figures 10 to 12a,b. From Figure 10, $\theta_0$ decreases considerably as $\lambda$ rises tenfold from 0.2 to 2.0, $Ec$ being fixed at 0.3. The Keller-Box and DSRK profiles are virtually indistinguishable implying excellent agreement for these two numerical schemes. Velocity function $f_1'$ decreases with $\lambda$ for a given $Ec$ value of 0.5. $\theta_1$, however, increases in magnitude greatly as $\lambda$ rises from 0.02 to 0.04. The values for $\theta_1$, are also higher for $Ec = 0.5$ than for $Ec = 0.0$, i.e. viscous dissipation has a positive effect

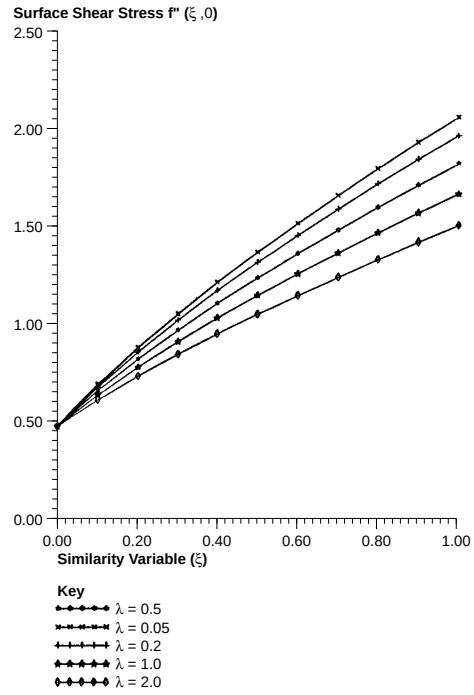


**Figure 3a.**
Variation of $V$ i.e. $f''(\xi,0)$ and $G(\xi,0)$ i.e. $\theta'(\xi,0)$ with streamwise coordinate $\xi$ at the plate surface ($\eta = 0$) for various thermal conductivity ratios ($\lambda$); results for Keller box scheme: $\alpha = 1.0$, $Gr = 100$, $Re = 1.0$, $Da = 0.05$, $Pr = 0.71$, $Ec = 0.3$

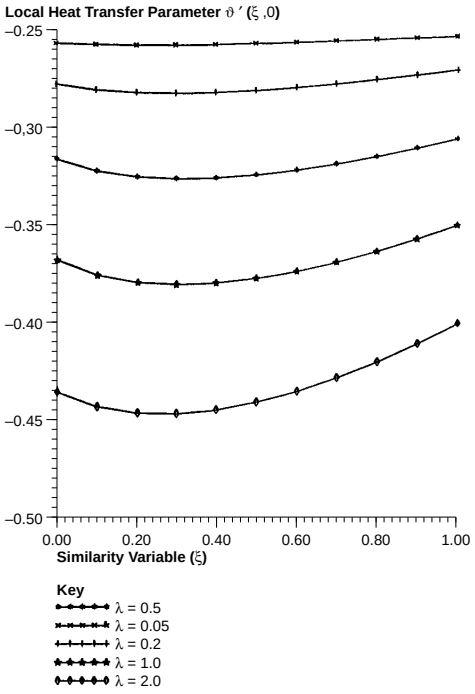


**Figure 3b.**
Variation of $V$ i.e. $f''(\xi,0)$ and $G(\xi,0)$ i.e. $\theta'(\xi,0)$ with streamwise coordinate $\xi$ at the plate surface ($\eta = 0$) for various thermal conductivity ratios ($\lambda$); results for Keller box scheme: $\alpha = 1.0$, $Gr = 100$, $Re = 1.0$, $Da = 0.05$, $Pr = 0.71$, $Ec = 0.3$

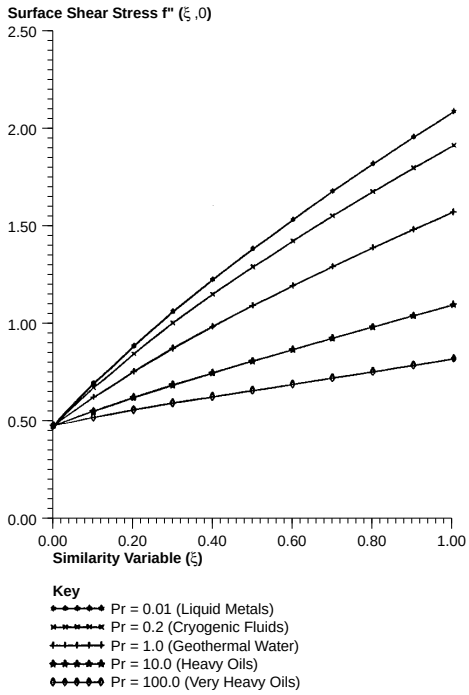


**Figure 4a.**
Variation of $V$ i.e. $f^{//}(\xi,0)$ and $G(\xi,0)$ i.e. $\theta'(\xi,0)$ with streamwise coordinate $\xi$ at the plate surface ($\eta = 0$) for various Prandtl numbers ($Pr$); results for Keller box scheme: $\alpha = 1.0$, $Gr = 100$, $Re = 1.0$, $Da = 0.05$, $Ec = 0.2$, $\lambda = 1.0$

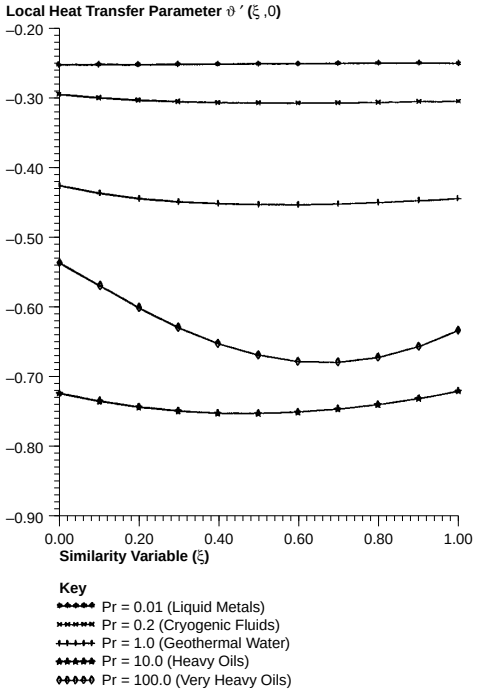


**Figure 4b.**
Variation of $V$ i.e. $f^{//}(\xi,0)$ and $G(\xi,0)$ i.e. $\theta'(\xi,0)$ with streamwise coordinate $\xi$ at the plate surface ($\eta = 0$) for various Prandtl numbers ($Pr$); results for Keller box scheme: $\alpha = 1.0$, $Gr = 100$, $Re = 1.0$, $Da = 0.05$, $Ec = 0.2$, $\lambda = 1.0$

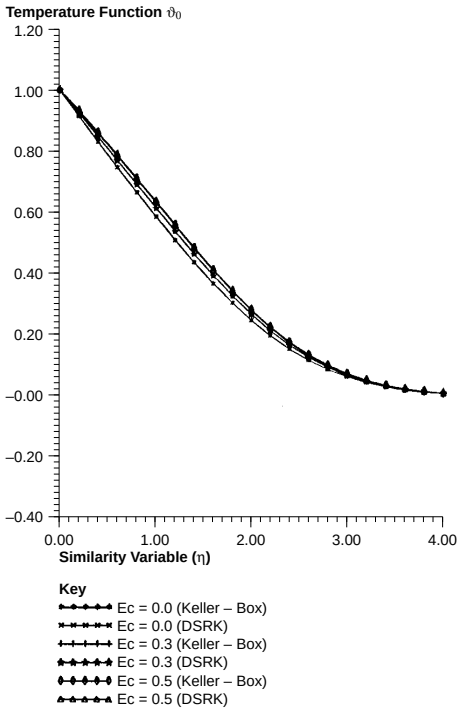


**Figure 5.**
Variation of $\theta_0(\eta)$ with spanwise coordinate $\eta$ for $\xi = 0$; results generated by DSRK scheme and Keller box for various Eckert numbers ($Ec$): $\alpha = 1.0$, $Pr = 0.71$, $\lambda = 1.0$

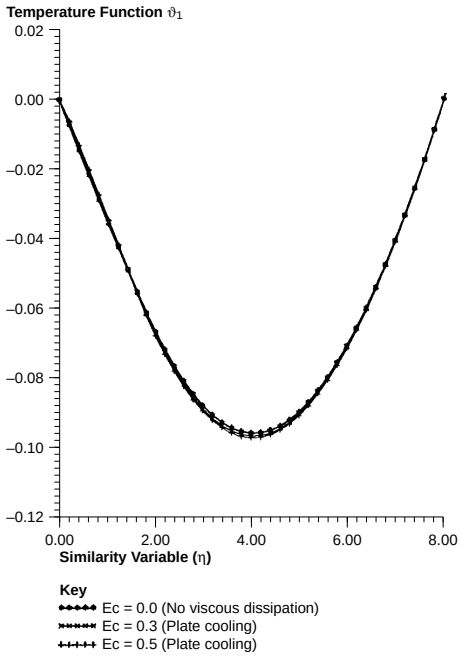


**Figure 6.**
Variation of $\theta_1(\eta)$ with spanwise coordinate $\eta$ for $\xi = 0$; results generated by DSRK scheme for various Eckert numbers ($Ec$): $\alpha = 1.0$, $Pr = 0.71$, $\lambda = 0.02$, $Re/GrDa = 0.2$

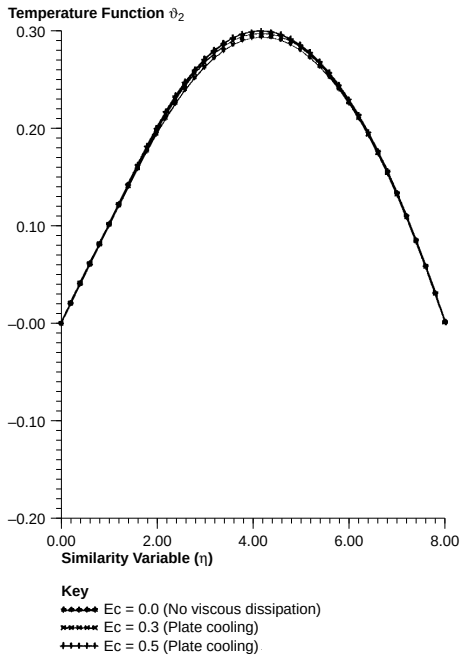


**Figure 7.**
Variation of $\theta_2(\eta)$ with spanwise coordinate $\eta$ for $\xi = 0$; results generated by DSRK scheme for various Eckert numbers ($Ec$): $\alpha = 1.0$, $Pr = 0.71$, $\lambda = 0.02$, $Re/GrDa = 0.2$

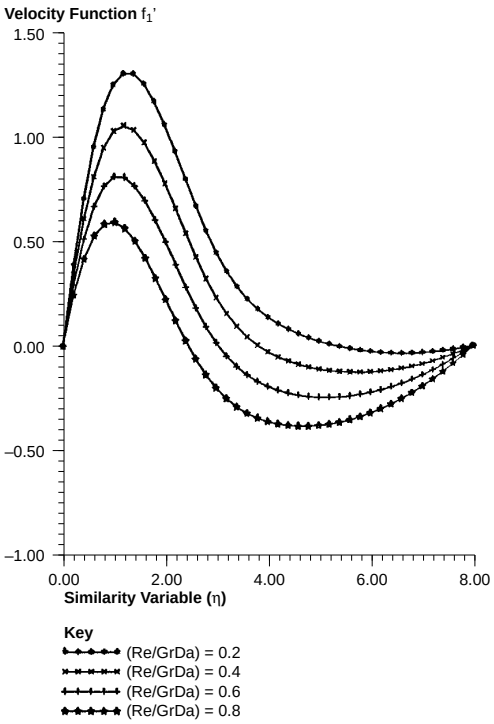


**Figure 8a.**
Variation of $f_1'(\eta)$ and $\theta_1(\eta)$ with spanwise coordinate $\eta$; results generated by DSRK scheme for various Darcy parameters ($Re/GrDa$): $\alpha = 1.0$, $Pr = 0.71$, $\lambda = 0.02$, $Ec = 0.3$

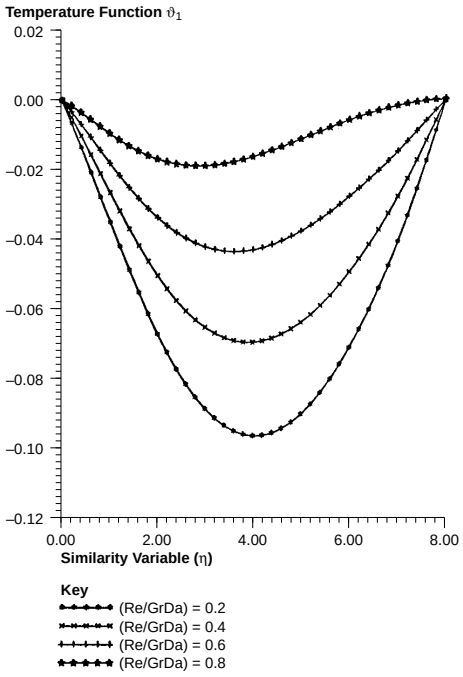


**Figure 8b.** Variation of $f_1'(\eta)$ and $\theta_1(\eta)$ with spanwise coordinate $\eta$; results generated by DSRK scheme for various Darcy parameters ($Re/GrDa$): $\alpha = 1.0$, $Pr = 0.71$, $\lambda = 0.02$, $Ec = 0.3$

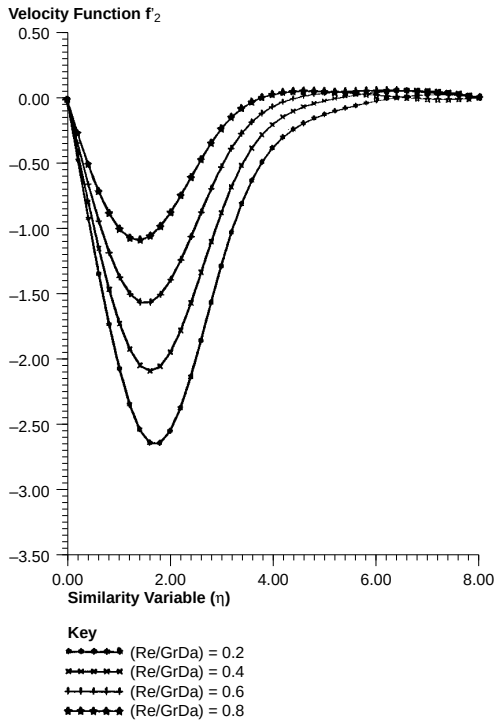


**Figure 9a.** Variation of $f_2'(\eta)$ and $\theta_2(\eta)$ with spanwise coordinate $\eta$: results generated by DSRK scheme for various Darcy parameters ($Re/GrDa$): $\alpha = 1.0$, $Pr = 0.71$, $\lambda = 0.02$, $Ec = 0.3$

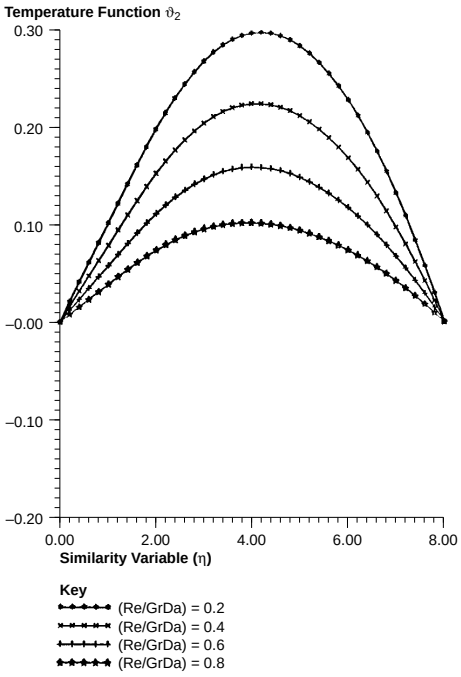


**Figure 9b.**
Variation of $f_2'(\eta)$ and $\theta_2(\eta)$ with spanwise coordinate $\eta$: results generated by DSRK scheme for various Darcy parameters ($Re/GrDa$): $\alpha = 1.0$, $Pr = 0.71$, $\lambda = 0.02$, $Ec = 0.3$

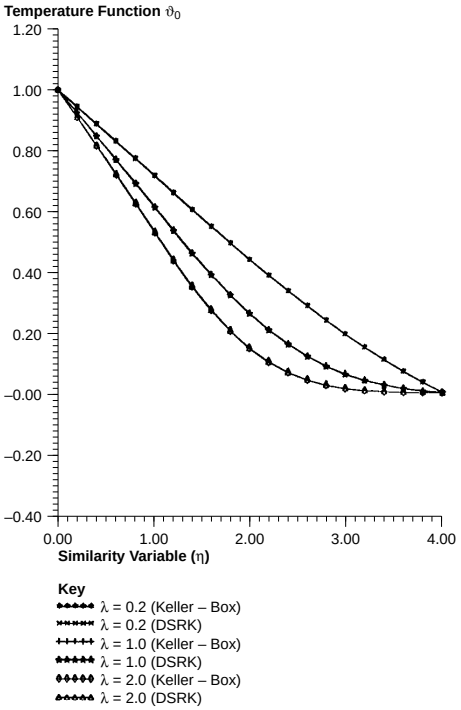


**Figure 10.**
Variation of $\theta_0(\eta)$ with spanwise coordinate $\eta$ for $\xi = 0.0$; results generated by DSRK scheme and Keller-box for various thermal condctivity ratios ($\lambda$): $\alpha = 1.0$, $Pr = 0.71$, $Ec = 0.3$

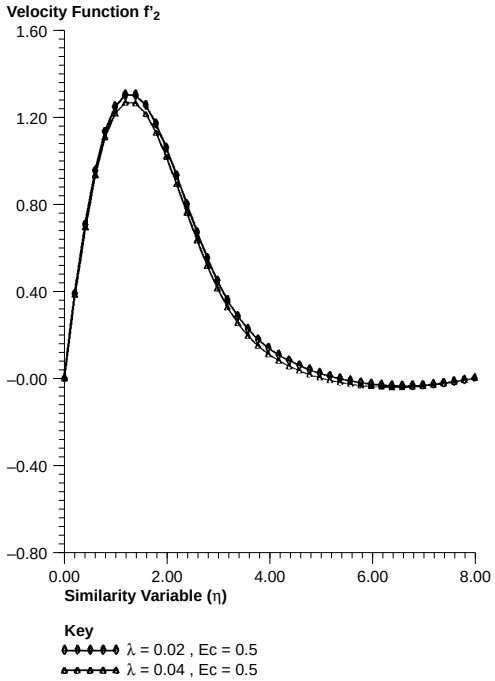


**Figure 11a.** Variation of $f_1'(\eta)$ and $\theta_1(\eta)$ with spanwise coordinate $\eta$; results generated by DSRK scheme for thermal conductivity ratios ($\lambda$): $\alpha = 1.0$, $Pr = 0.71$, $Re/GrDa = 0.2$

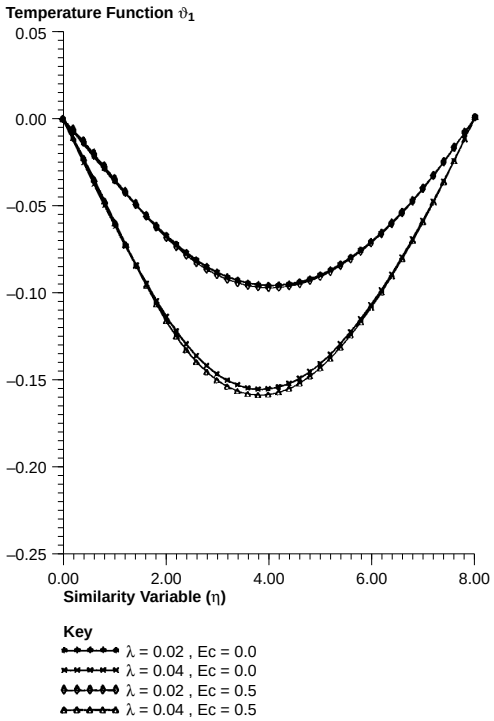


**Figure 11b.** Variation of $f_1'(\eta)$ and $\theta_1(\eta)$ with spanwise coordinate $\eta$; results generated by DSRK scheme for thermal conductivity ratios ($\lambda$): $\alpha = 1.0$, $Pr = 0.71$, $Re/GrDa = 0.2$

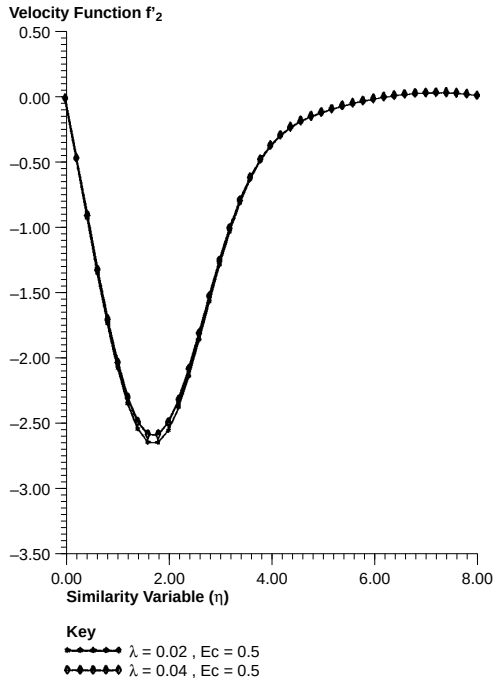


**Figure 12a.**
Variation of $f_2'(\eta)$ and $\theta_2(\eta)$ with spanwise coordinate η; results generated by DSRK scheme for thermal conductivity ratios ($\lambda$): $\alpha = 1.0$, $Pr = 0.71$, $Re/GrDa = 0.2$

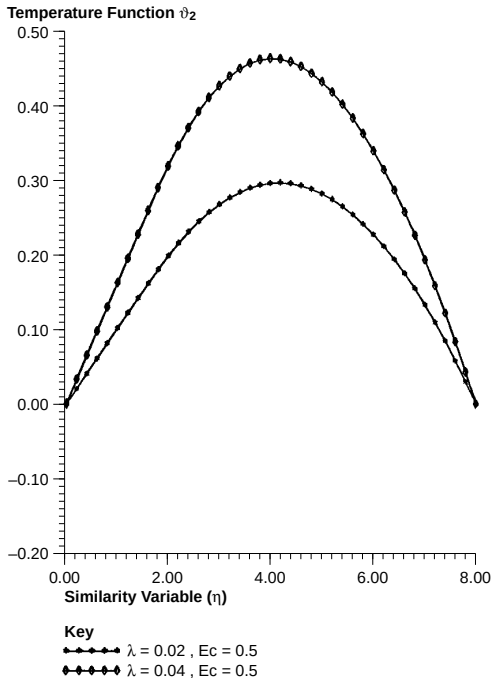


**Figure 12b.**
Variation of $f_2'(\eta)$ and $\theta_2(\eta)$ with spanwise coordinate $\eta$; results generated by DSRK scheme for thermal conductivity ratios ($\lambda$): $\alpha = 1.0$, $Pr = 0.71$, $Re/GrDa = 0.2$

on the magnitude of $\theta_1$. The second order function profiles for $f_2'$ and $\theta_2$, are shown in Figures 12a,b. $f_2'$ magnitudes are decreased slightly as $\lambda$ rises from 0.02 to 0.04 with $Ec$ fixed at 0.5. Temperature $\theta_2$ is, however, greatly increased as $\lambda$ rises from 0.02 to 0.04.

Figure 13 shows the variation of the zero order temperature $\theta_0$ function with the spanwise coordinate $\eta$ for various Prandtl numbers obtained with the double shooting Runge Kutta method (DSRK) and Keller-Box scheme. As $Pr$ is increased from 0.01 (liquid metals) to 1.0 and then 10.0, a large fall in temperature is induced since larger Prandtl number fluids have lower thermal diffusivites for a given viscosity and therefore less thermal energy is transported. Both Keller-Box and DSRK computations are practically identical again, reflecting the excellent accuracy of the Keller finite-difference scheme.

Observing Figures 14a,b and 15a,b, first order velocity $f_1'$ is increased slightly in magnitude as $Pr$ falls from 0.71 designating air to 0.2[35], which is of the range for most refrigerant or cryogenic fluids used in industry and certain geothermal gases. First order temperature function $\theta_1$ is similarly increased positively (although effectively the magnitude falls) by reduction in the Prandtl number. Finally second order velocity $f_2'$ and temperature function $\theta_2$ are

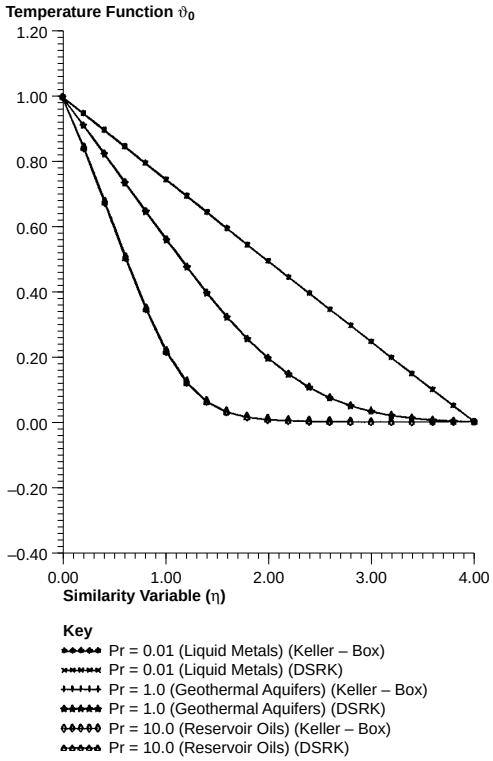


**Figure 13.**
Variation of $\theta_0(\eta)$ with spanwise coordinate $\eta$ for $\xi = 0$; results generated by DSRK scheme and Keller-box method for various Prandtl numbers ($Pr$): $\alpha = 1.0$, $\lambda = 1.0$, $Ec = 0.2$

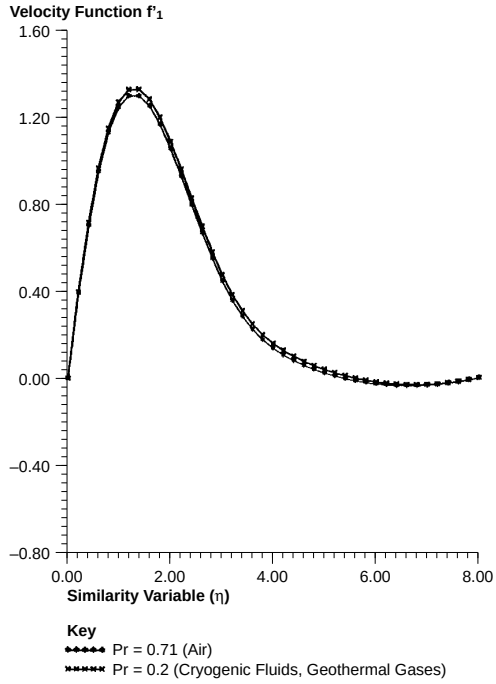


**Figure 14a.**
Variation of $f_1'(\eta)$ and $\theta_1(\eta)$ with spanwise coordinate $\eta$; results generated by DSRK scheme for various Prandtl numbers (*Pr*): $\alpha = 1.0$, $\lambda = 0.02$, *Ec* = 0.0, *Re*/*GrDa* = 0.2

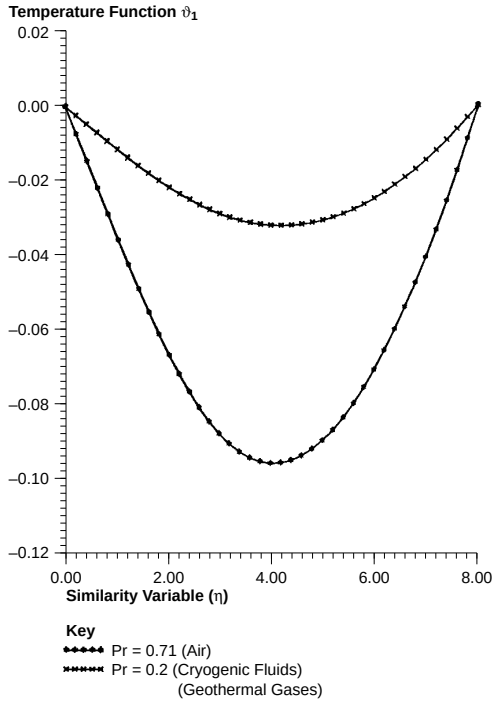


**Figure 14b.**
Variation of $f_1'(\eta)$ and $\theta_1(\eta)$ with spanwise coordinate $\eta$; results generated by DSRK scheme for various Prandtl numbers (*Pr*): $\alpha = 1.0$, $\lambda = 0.02$, *Ec* = 0.0, *Re*/*GrDa* = 0.2

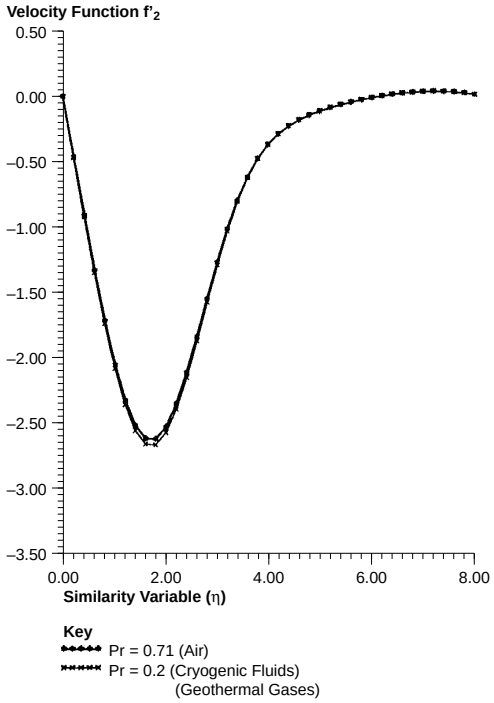


**Figure 15a.** Variation of $f_2'(\eta)$ and $\theta_2(\eta)$ with spanwise coordinate $\eta$; results generated by DSRK scheme for various Prandtl numbers ($Pr$): $\alpha = 1.0$, $\lambda = 0.02$, $Ec = 0.0$, $Re/GrDa = 0.2$

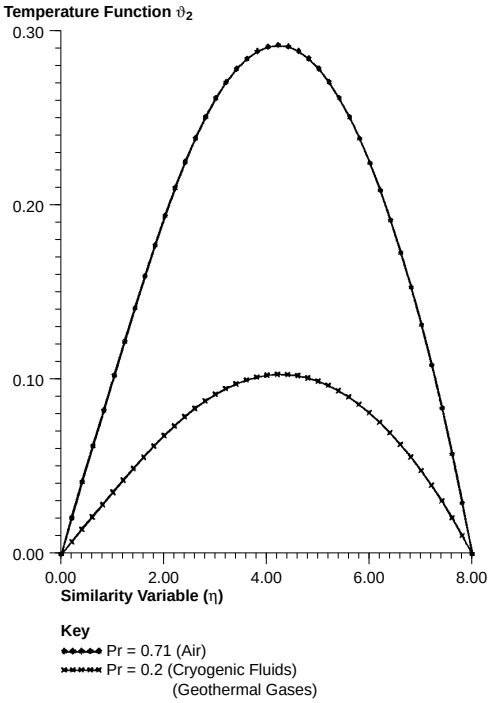


**Figure 15b.** Variation of $f_2'(\eta)$ and $\theta_2(\eta)$ with spanwise coordinate $\eta$; results generated by DSRK scheme for various Prandtl numbers ($Pr$): $\alpha = 1.0$, $\lambda = 0.02$, $Ec = 0.0$, $Re/GrDa = 0.2$

respectively increased slightly in magnitude and decreased considerably as *Pr* is lowered from 0.71 to 0.2.

## Concluding remarks

Buoyancy-induced two dimensional convective boundary layer flow past a flat vertical plate embedded in a homogeneous, isotropic, saturated porous medium has been analysed using the Darcy-Brinkman porous model, a pseudo-similarity transformation and numerical techniques. It has been shown that local shear stresses at the plate are enhanced with increasing *Da* and *Ec* values and conversely depressed with rising $\lambda$ and *Pr* values. Rising $\lambda$, *Pr* and *Da* all elevate local heat transfer magnitudes. Heat transfer is, however, reduced with increasing *Ec* since this corresponds to cooling of the plate, i.e. loss of thermal energy.

### References

1. Domenico, P.A. and Schwartz, F.W., *Physical and Chemical Hydrogeology,* John Wiley & Sons, New York, NY, 1990.
2. Cheng, P., "Geothermal heat transfer", in Rohsenhow, W.M. *et al.* (Eds), *Handbook of Heat Transfer Applications,* 2nd edition, Chapter 11, McGraw-Hill, New York, 1985.
3. Kim, W-S. and Tarbell, J.M., "Macromolecular transport through the deformable porous media of an artery wall", ASME *J. Biomechanical Engineering,* Vol. 116, 1994, pp. 156-163.
4. Nakayama, A. and Hossain, M.A., "Free convection in a saturated porous medium beyond the similarity solution", *Applied Scientific Research,* Vol. 52, 1994, pp. 133-45.
5. Lowell, R.P., "Topographically driven subcritical hydrothermal convection in the oceanic crust", *Earth Planetary Sci. Lett.,* Vol. 49, 1980, pp. 21-8.
6. King, P.R. (Ed.), *Mathematics of Oil Recovery*, IMA Press, 1992.
7. Combarnous, M.A. and Bories, S.A., "Hydrothermal convection in saturated porous media", *Advances in Hydroscience,* Vol. 10, 1975, pp. 231-307.
8. Adler, P., *Porous Media: Geometry and Transports,* Butterworths, 1992.
9. Whitaker, S., "Theory of filtration in porous media", *Advances in Heat Transfer,* 1987.
10. Duffie, J.A. and Beckman, W.A., *Solar Engineering of Thermal Processes,* John Wiley, New York, NY, 1980.
11. Bear, J., *Dynamics of Fluids in Porous Media,* Dover, New York, NY, 1988.
12. Brinkman, H.C., "A calculation of the viscous forces exerted by a flowing fluid on a dense swarm of particles", *Applied Scienctific Research,* 1947, A1, pp. 27-34.
13. Bear, J. and Bachmat, Y., *Introduction to Modelling of Transport Phenomena in Porous Media,* Kluwer, 1990.
14. Nield, D.A., "The boundary correction for the Rayleigh-Darcy problem: limitations of the Brinkman equation", *J. Fluid Mechanics,* Vol. 128, 1983, pp. 37-46.
15. Nield, D.A. and Bejan, A., *Convection in Porous Media,* Springer-Verlag, New York, NY, 1992.
16. Lundgren,T.S., "Slow flow through stationary random beds and suspensions of spheres", *J. Fluid Mechanics,* Vol. 51, 1972, pp. 273-99.
17. Durlofsky, L. and Brady, J.F., "Analysis of the Brinkman equation as a model for flow in porous media", *Physics of Fluids,* Vol. 30, 1987, pp. 3329-41.
18. Beavers, G.S. and Joseph, D.D., "Boundary conditions at a naturally permeable wall", *J. Fluid Mechanics,* Vol. 30, 1967, pp. 197-207.

19. Kaviany, M., *Principles of Heat Transfer in Porous Media,* McGraw-Hill Book Company, New York, NY, 1991.
20. Prasad, V. and Kladias, N., "Non-Darcy natural convection in saturated porous media", in Kakac, S., Kilkis, B., Kulacki, F.A. and Arinc, F. (Eds), *Convective Heat and Mass Transfer in Porous Media,* Kluwer Academic, NATO Series in Applied Science, Dordrecht, 1991.
21. Evans, G.H. and Plumb, O.A., "Natural convection from a vertical isothermal surface embedded in a saturated porous medium". AIAA-ASME *Thermophysics and Heat Transfer Conference,* paper 78-HT-55, 1978, Palo Alto, CA, USA.
22. Ganapathy, R. and Purushothaman, R., "Thermal convection from an instantaneous point heat source in a porous medium", *Int. J. Engineering Science,* Vol. 28, 1990, pp. 907-18.
23. Sen, A.K., "Natural convection in a shallow porous cavity – the Brinkman model", *Int. J. Heat Mass Transfer,* Vol. 30, 1987, pp. 855-68.
24. Vasseur, P. and Robillard, L., "The Brinkman model for boundary layer regime in a rectangular cavity with uniform heat flux from the side", *Int. J. Heat and Mass Transfer,* Vol. 30, 1987, pp. 717-28.
25. Tong, T.W. and Subramanian, E., "A boundary layer analysis for natural convection in vertical porous enclosures – use of the Brinkman-extended Darcy model", *Int. J. Heat Mass Transfer*, Vol. 28, 1985, pp. 563-71.
26. Tong, T.W. and Orangi, S., "A numerical analysis for high modified Rayleigh number natural convection in enclosures containing a porous medium", *Heat Transfer 1986,* Hemisphere, Washington, DC, Vol. 5, 1986, pp. 2647-52.
27. Takhar., H.S., Soundalgekar, V.M. and Gupta, A.S., "Mixed convection of an incompressible fluid in a porous medium past a hot vertical plate", *Int. J. Non-Linear Mechanics*, Vol. 25 No. 6, 1990, pp. 723-8.
28. Parang, M. and Keyhani, M., "Boundary effects in laminar mixed convection flow through an annular porous medium", *ASME Journal Heat Transfer,* Vol. 109, 1987, pp. 1039-41.
29. Cebeci, T. and Bradshaw, P., *Physical and Computational Aspects of Convective Heat Transfer,* Springer-Verlag, Berlin, 1984.
30. Keller, H.B., *Numerical Solution of Two Point Boundary Value Problems*, SIAM Press, Philadelphia, 1976.
31. Gorla, R.S.R., "Radiative effects on conjugate forced convection in a laminar wall jet along a flat plate", in Chereminisoff, N. (Ed.), *Encyclopedia of Fluid Mechanics, Advances in Flow Dynamics,* Supplement 3, Chapter 22, 1994.
32. Bèg, Ò.À., Takhar, H.S. and Kumari, M., "Non-similar hydromagnetic thermoconvection flow of a viscoelastic second order non-Newtonian fluid past a horizontal wedge embedded in a porous medium", submitted to *International J. Non-Linear Mechanics,* November 1997.
33 Bèg, Ò.À., "Non-Darcy thermoconvective hydrodynamic flows through porous media with magnetohydrodynamic and radiative effects", PhD thesis in Numerical Hydrodynamics, School of Engineering, University of Manchester, March 1996.
34. Gorla, R.S.R. and Takhar, H.S., "Combined convective heat transfer from a flat plate embedded in porous media", *Int. J. Eng. Fluid Mech,* Vol. 4, 1991, pp. 363-73.
35. Holman, J.P., *Heat Transfer,* 7th ed., McGraw-Hill, New York, NY, 1992.